RSC Advances RSC Publishing

COMMUNICATION

Cite this: DOI: 10.1039/x0xx00000x

Cu-MoS_2-ITO based hybrid structure for catalysis of hydrazine oxidation

Sajjad Hussain[a,b], Kamran Akbar[c], Dhanasekaran Vikraman[a,b], Muhmmad Arslan Shehzad[a,b], Seunho Jung [c], Yongho Seo[a,b], and Jongwan Jung[*a,b]

Received 00th January 2012,
Accepted 00th January 2012

DOI: 10.1039/x0xx00000x

www.rsc.org/advances

We have successfully demonstrated large-area and continuous MoS_2 films grown onto indium tin oxide (ITO) substrates by RF sputtering followed by post-annealing process. Thin Cu layers were prepared onto MoS_2/ITO film by thermal evaporation to enhance electron-transfer rates as well as the catalytic activity of hydrazine oxidation. High electrocatalytic activity towards the hydrazine oxidation was observed in a Cu-MoS_2-ITO hybrid structure. A large residual current was also observed in the Cu-MoS_2-ITO hybrid due to the combination of MoS_2 and Cu film. The electrocatalytic activity was enhanced with the increase of the MoS_2 film thickness. The observed results showed that the Cu-MoS_2-ITO catalyst is indeed a valuable material for future applications in hydrazine fuel cells.

Introduction

In recent years, layered transition metal dichalcogenides (LTMDs) have been the focus of many studies due to their distinctly unique properties such as high mobility and high current on/off ratio[1], high mechanical strength and stability in inert atmosphere[2-4]. Molybdenum disulfide (MoS_2), a representative LTMD member, has many advantages as well, including low cost, earth-abundance, high chemical stability and outstanding photocatalytic activity as well as potential electrocatalytic properties in hydrogen evolution reaction (HERs)[5-9]. Basically, MoS_2 consists of two-dimensional sheets of vertically stacked S−Mo −S interlayers linked together by weak Vander-Waals forces. The most important feature in this LTMD family of materials is the body thickness scalability down from bulk (indirect band gap of 1.3 eV) to a monolayer (direct band gap of 1.8 eV). Much effort has been put forth to investigate the catalytic activities of MoS_2, and MoS_2/graphene heterostructures[10,11]. Both the theoretical and experimental results of previous studies have confirmed that the catalytic activity of MoS_2 originates from the reactive sulfur edges[12-14]. Electrocatalytic activity is highly dependent on the catalyst morphology, grain size, surface texture, crystalline structure and electrical conductivity. Thus, thin MoS_2 with exposed edges becomes more active for electrocatalysis than the bulk forms of materials [12, 13].

Recently, many studies have been performed with the aim to enhance the electrocatalytic activity of liquid-feed fuel cells using fuel such as ethylene glycol[15], sodium borohydride[16] and hydrazine[17]. Among them, hydrazine (N_2H_4) is a high-energy fuel molecule that has received considerable attention. Many studies have been done to improve electrocatalytic activity using graphene oxide (GO) or carbon nanotubes (CNTS). Li et al.[18,19] have demonstrated high electrocatalytic activity toward hydrazine oxidation using Ni-Fe alloy on polyethyleneimine (PEI)-functionalized graphene oxide (GO) electrocatalyst. Ye et al.[20] have reported electrocatalytic activity of Pd–Ni/CNT. Graphene-like MoS_2 also can provide abundant active edges for potential catalytic performance and a large specific surface area for catalytic support. Zhong et al.[21] have reported that Ni–Fe/MoS_2 hybrid by in-situ growth of a Ni-Fe alloy, exhibited high electrocatalytic activity toward hydrazine oxidation.

In this work we used sputtered few-layer MoS_2 on indium tin oxide (ITO) and studied the catalytic activity of hydrazine oxidation. To enhance the electrocatalytic activity toward hydrazine oxidation, a thin Cu layer (~ 2 nm) was coated onto MoS_2/ITO film by a thermal evaporation system in a high vacuum (an order of 10^{-7} torr) with a deposition rate of 1.0 Å/s and the thickness was monitored during the deposition by a quartz oscillator. The thin Cu layer improves the electron-transfer rates and enhances the catalytic activity of hydrazine oxidation through the synergistic effects of the Cu and MoS_2/ITO. ITO substrate has many advantages such as low cost, excellent optical transparency, high electrical conductivity, wide electrochemical working window, stable electrochemical and physical properties[22-26]. Many previous reports based on ITO used as a substrate for electrocatalytic activity[27] are also available. The hybrid structure used is shown in Figure 1(a). To date, many researchers have paid attention to growing MoS_2 film via RF magnetron sputtering on fluorine-doped tin oxide (FTO), silicon and glass sheet substrates[28, 29]. However, to the best of our knowledge, our work is the first to study the electrocatalysis of hydrazine oxidation of continuous few-layer MoS_2 sputtered on ITO.

Experimental and Device Fabrication Details

ITO substrates were ultrasonically degreased by immersion in acetone, methanol, isopropyl alcohol (IPA) and deionized (DI) water and then baked at 120°C for 5 minutes. Initially, MoS_2 thin films were deposited by RF magnetron sputtering. The high pure (99.96%) MoS_2 target was used for the deposition of films. The vacuum coating unit was initially evacuated to a base pressure of $\sim 1\times 10^{-7}$ torr and argon (Ar) gas was primarily allowed to flow into the chamber for 5 minutes in order to remove the oxide layer on the surface of the target. During the film depositions, the Ar flow ratio was maintained at 10 sccm and the RF power was fixed at 50 W. The films were sputtered initially at room temperature at four different deposition times (1, 3, 5 and 10 minutes). We have used a shadow mask to sputter MoS_2 only on a specific area of the whole substrate. The sputtered MoS_2 thin films were subjected to annealing by sulfurization process at 600°C under an Ar environment for 1 hour. Sulfur powder (99.99% purity) of 0.3 g, placed upstream in the chamber, was evaporated at 120 °C with Ar (100 sccm) as a carrier gas and the pressure of the CVD chamber was kept at 2 $x10^{-2}$ torr. The electrocatalytic activity of the Cu/MoS_2/ITO hybrid was systematically investigated through cyclic voltammetry in 75 mM NaOH with 0.1 mM hydrazine hydrate using a three-electrode setup which consists of saturated Ag/AgCl as the reference electrode, a platinum wire as the counter electrode and Cu/MoS_2/ITO hybrid as the working electrode.

Results and Discussion

Figure 1(b-e) shows the optical microscopy (OM) images of MoS_2/ITO and Cu/MoS_2/ITO. We have intentionally covered one portion of the films in order to enhance the contrast of the images from which the films were observed to be continuous and uniform over a large area.

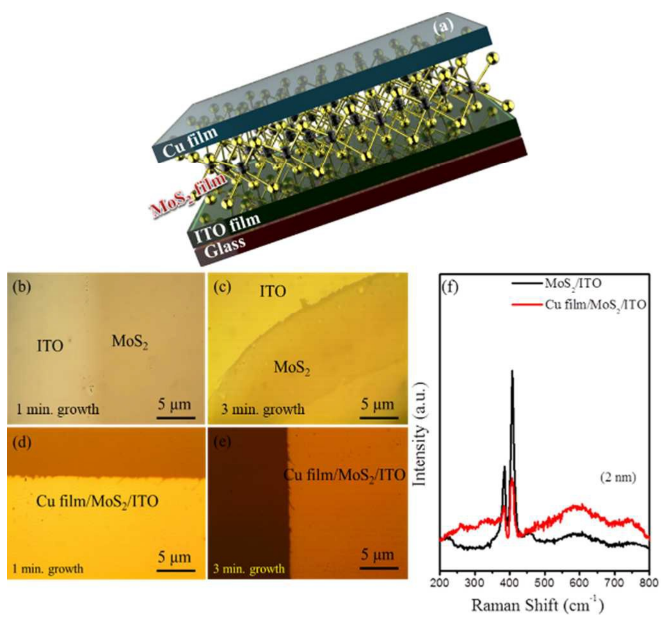

Figure 1 (a) A schematic view of Cu/MoS_2/ITO hybrid structure; **(b,c)** Optical images of MoS_2/ITO films. They were sputtered for 1 and 3 minutes onto ITO substrates and annealed in Ar and sulfur environment at 600°C; **(d,e)** Optical images of Cu/MoS_2/ITO hybrid structures prepared using MoS_2 films; **(f)** Raman spectra of MoS_2/ITO (black line) and Cu/MoS_2/ITO (red line).

Raman analysis was performed to investigate the structure of MoS_2 nanosheets and to identify the number of MoS_2 layers [30, 31]. Raman spectra of MoS_2/ITO and Cu/MoS_2/ITO hybrid structure are shown in **figure 1 (f)**. The strong Raman peaks are observed at 383.9 and 405.3 cm^{-1} for 1 minute-MoS_2 (~ 2 nm) and they have associated with the in-plane vibrational (E_{2g}^1) and out-of-plane vibrational (A_{1g}) modes, respectively. The peak separation (Δk) between (E_{2g}^1) and (A_{1g}) mode is approximately 21.4 cm^{-1}, which is in good agreement with that of 2-3 layers of MoS_2 [30,32,33]. The peak separation was also confirmed by Raman mapping analysis as shown in figure S1. Raman mapping was performed over an area of 30 µm × 30 µm of the MoS_2 film (1 minute-sample). The E_{2g}^1 mode appeared at 382-384 cm^{-1} and the A_{1g} mode at 404.5-406.5 cm^{-1}. The Δk values are located in the range of ~20–22 cm^{-1}, confirming 2-3 layers of MoS_2 [32]. The Δk value increases to ~25, ~26.5 and ~30.9 cm^{-1}, for the sputtering time of 3, 5 and 10 minutes, respectively in figure 2(e-g). Thus, Raman spectra clearly supports that the MoS_2 film becomes thicker with increasing sputtering time. It can be noted that E^1_{2g} mode and A_{1g} vibrational modes decreases and broadens but no noticeable changes in peak position are observed after deposition of Cu film. For the thickness of the MoS_2 film, an AFM scan was taken from the corner of the MoS_2 film patterned using a shadow mask. The estimated film thickness is ~ 2 nm for 1 minute-MoS_2 (sputtering time of 1 minute), as shown in figure 2a, corresponding to 2-3 layers of MoS_2 [34]. The thickness increases to ~ 5, ~7, and ~10 nm for 3, 5, 10 minutes, respectively as shown in figure 2 (b-d). Thus, the film thickness of MoS_2 is controllable by tuning the sputtering time. Surface morphological and topographical images of MoS_2/ITO and Cu/MoS_2/ITO hybrid structures (2 nm-thick MoS_2) are shown in figure 3 (a-d). AFM topographical image represents the nanocrystalline structures of MoS_2/ITO.

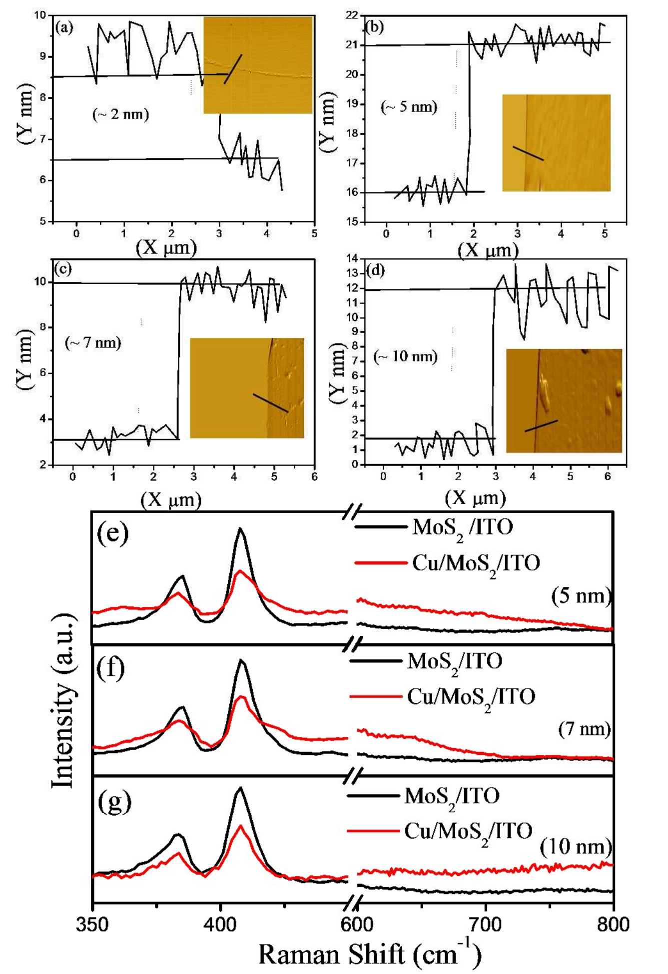

Figure 2 AFM height profiles for MoS_2 films with different thickness, **(a)** ~2 nm **(b)** ~5 nm **(c)** ~7 nm and **(d)** ~10 nm. Inset: AFM topological image of the corresponding film; **(e-g)** Raman spectra of MoS_2/ITO and Cu/MoS_2/ITO hybrid structures with different thickness of MoS_2 films (5 nm, 7 nm and 10 nm).

The X-ray diffraction (XRD) patterns of MoS_2/ITO and Cu/MoS_2/ITO hybrid structures are shown in figure 3 (e-f). For the MoS_2/ITO structure, the MoS_2-related peaks are observed at 2θ = 14.18°, 33.57° and 70.01° which are consistent with bulk MoS_2 (JCPDS card no. 37-1492) having a hexagonal phase with $P6_3/mmc$ (194) space group. And, substrate-related minor peaks are also observed at 22.5°, 32.5° and 45.5°, corresponding to the (222), (400) and (440) reflections, respectively. For the Cu/MoS_2/ITO hybrid structure, the diffraction peaks of Cu (2θ =43.38 and 50.48) appeared. The MoS_2-related peaks of (002) and (201) and ITO-related peaks are highly suppressed and couple of Cu-related peaks are emerged in Cu/MoS_2/ITO hybrid structure as shown in figure 3(f).

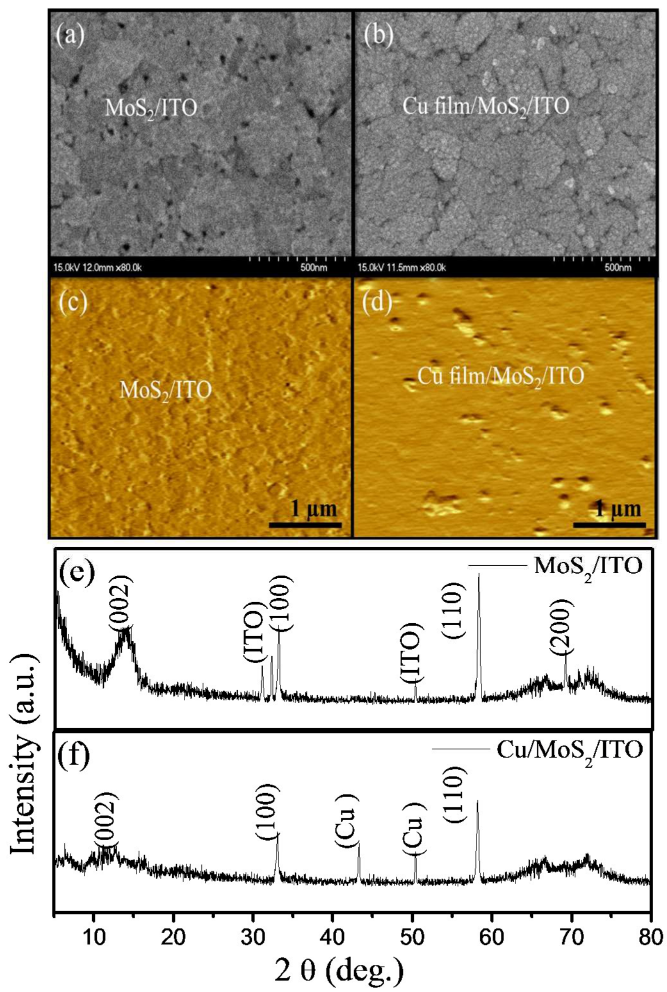

Figure 3. SEM micrographs, 2D-AFM topographs and XRD patterns of MoS_2/ITO and Cu/MoS_2/ITO hybrid structures .

To evaluate the electrocatalytic activity, cyclic voltammetry was investigated for MoS_2/ITO, Cu/ITO and Cu/MoS_2/ITO hybrid in 75 mM NaOH with 0.1mM Hydrazine aqueous solutions at the scan rate of 100 mV/sec (figure 4).

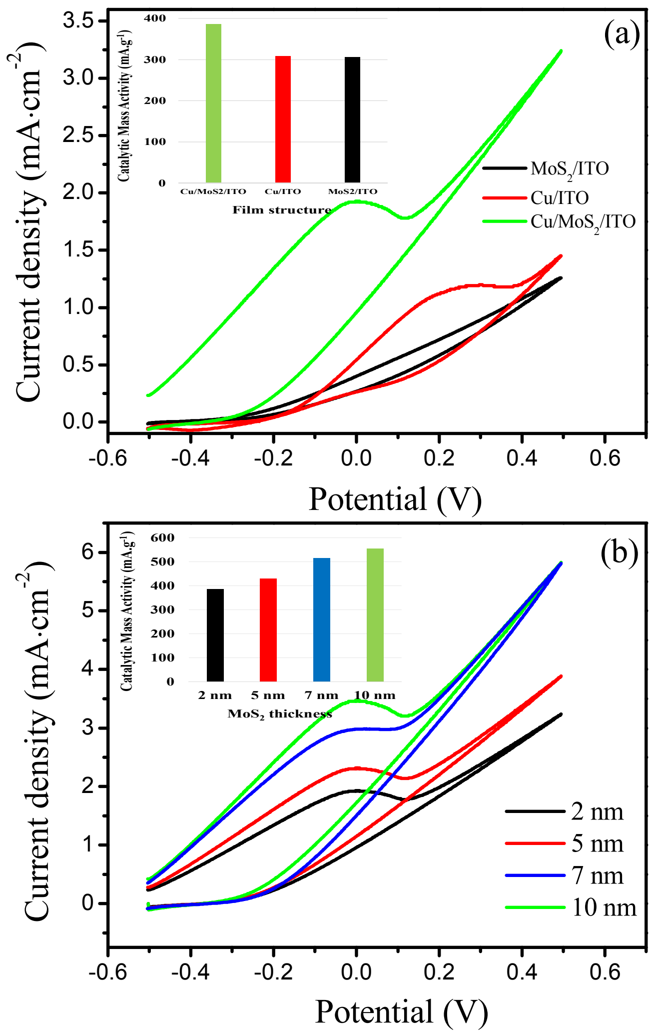

Figure 4 (a) Cyclic voltammetry of MoS_2/ITO, Cu/ITO and Cu/MoS_2/ITO hybrid structures at a scan rate of 100 mV/sec; (b) Cyclic voltammetry of Cu/MoS_2/ITO hybrid structures with different thickness (2-10 nm) of MoS_2 layer at a scan rate of 100 mV/sec.

It can be seen that the bare MoS_2 film on ITO (MoS_2/ITO) does not exhibit any hydrazine oxidation peak while the Cu-coated ITO electrode (MoS_2/ITO) exhibits a small electrocatalytic activity peak towards hydrazine oxidation (figure 4a). The observed current density value is 1.19 $mA\cdot cm^{-2}$ for Cu/ITO electrode. The maximum peak current is observed at 1.93 $mA\cdot cm^{-2}$ for the Cu/MoS_2/ITO hybrid, which represented the maximum electrocatalytic activity towards hydrazine oxidation. Yang et al.[35] reported up to 950 $\mu A\cdot cm^{-2}$ current density value for Ag/CNT composites in 0.1 M K_2SO_4 electrolyte solution with 10 mM hydrazine, which is quite low compared with our observed results. The catalytic mass activity for different types of electrodes is plotted as shown in inset fig. 4(a). There is an overall negative shift of peak potential for Cu/MoS_2/ITO when compared to Cu/ITO, which reflects a fast electron-transfer reaction on Cu/MoS_2/ITO. Furthermore, the reverse scan gives no corresponding cathodic peak, suggesting a totally irreversible oxidation of hydrazine in alkaline solutions on Cu/MoS_2/ITO. The suggested mechanism of hydrazine oxidation on copper substrate is given as follows[36].

$$N_2H_4 + OH^- \rightarrow N_2H_3 + H_2O + e^- (slow)...........(a)$$

$$N_2H_3 + OH^- \rightarrow N_2 + 3H_2O + 3e^- (fast)..............(b)$$

This mechanism explains the irreversibility of the reaction and the absence of the cathodic peak because the formation of stable species such as nitrogen as an end product is difficult to reduce under the given voltages.

The cyclic voltammetry of the Cu/MoS_2/ITO hybrid with various thicknesses of MoS_2 is shown in figure 4b. The current value increased with the increase of MoS_2 layer thickness. The current density increased to 2.3, 3.0 and 3.4 $mA\cdot cm^{-2}$ for 5, 7 and 10 nm-MoS_2, respectively. Also the catalytic mass activity values are plotted for different MoS_2 layer thicknesses as shown in inset figure 4b. The highest mass catalytic activity of 555 $mA\cdot g^{-1}$ was obtained for Cu/MoS_2/ITO hybrid with 10 nm-thick MoS_2. Gao et al.[36] reported the current density of 14 $mA\cdot cm^{-2}$ using Cu nanotubes−graphene paper (Cu−GP) hybrid in 0.1 M KOH containing 10 mM hydrazine at a scan rate of 100 mV/s. The 106 μA were achieved for Pd/WO_3-ITO electrode by using 5 mM $N_2H_4SO_4$ solution[37]. Yi et al.[38] have reported significantly improved electrocatalytic activity (100 $mA\cdot cm^{-2}$) with Au/Ti electrode for hydrazine oxidation in alkaline solutions, in which the electrode was modified using a hydrothermal method. In our work, sputtered-MoS_2 film thickness plays an important role in the electrocatalytic activity for the oxidation of hydrazine. As mentioned in the introduction, MoS_2 provides the active edges for potential catalytic performance and also provides a large specific surface area for catalytic support [12-14]. Our results indicate that the electrocatalytic activity gradually increases with the thickness of few-layer MoS_2 in this thickness range (2~10 nm). There is a report that sputtered MoS_2 on insulator most likely contains some Mo-O interfacial layer due to Mo atoms bound to the O atoms of oxide, while further deposition results in a MoS_2 film with a lower oxygen content[39]. We also noticed the same tendency in our films. The Mo-O interfacial layer may hinder the catalytic activity of MoS_2. The catalytic activity dependence of MoS_2 film thickness may be attributed to the fact that as the MoS_2 thickness increases, the effect of the Mo-O interfacial layer decreases in this thickness range. Cyclic voltammetry measurements were performed at different scan rates in order to investigate the reaction mechanism of hydrazine oxidation at the Cu/MoS_2/ITO electrode as shown in figure 5a. The oxidation peak potential and peak current density as well as the catalytic mass activity increase with increasing scan rates as shown in fig. 5a. The oxidation peak current (I_p) for hydrazine is linearly proportional to the scan rate, which indicates that the electrochemical oxidation of hydrazine at the Cu/MoS_2/ITO electrode is an adsorption-limited process. The stability of the catalysts is of great importance for device fabrications. The multiple cycle voltammetry is presented in figure S2 for the stability confirmation. It shows a quite stable cyclic voltammetry up to 20 cycles. The chronoamperometric measurement was used to assess the durability of the catalysts. Figure S3 shows the I–t curves of the Cu/MoS_2/ITO hybrid and the Cu/ITO electrode at a working potential of -0.4 V. The larger residual current is observed in Cu/MoS_2/ITO hybrid compared with Cu/ITO hybrid, which indicates that the MoS_2 with Cu film offers superior electrocatalytic activity for hydrazine electro-oxidation.

Conclusion

We used few-layer MoS_2 on ITO and studied the catalytic activity of hydrazine oxidation. The MoS2 film was sputtered at room temperature and then post-annealed to improve the crystallinity. The number of layers in MoS_2 was estimated by Raman spectra and AFM measurement. The Cu/MoS_2/ITO hybrid exhibited an excellent electrocatalytic activity and stability toward hydrazine oxidation. The electrocatalytic activity enhanced with the increase of MoS_2 film thickness up to 10 nm. This novel approach shows that graphene-like MoS_2 is a promising support material for a variety of applications in synergistic catalysis.

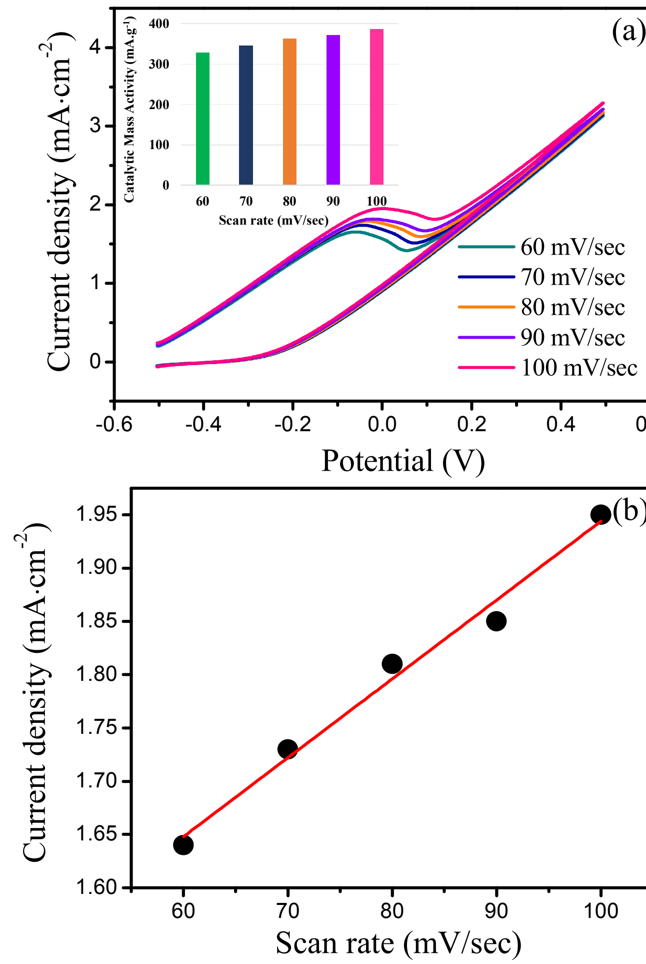

Figure 5 (a) Cyclic voltammetry of Cu/MoS_2/ITO hybrid structures performed at different scan rates; (b) I_p against scan rate plot of Cu/MoS_2/ITO hybrid electrode.

Acknowledgements

This research was supported by Basic Science Research Program through the National Research Foundation of Korea (NRF) funded by the Ministry of Education (2010-0020207, 2012R1A1A2007211).

Notes and references

[a] *Graphene Research Institute, Sejong University, Seoul 143-747, Republic of Korea*

[b] *Institute of Nano and Advanced Materials Engineering, Sejong University, Seoul 143-747, Republic of Korea*

[c] *Center for Biotechnology Research in UBITA (CBRU), Dept. of Bioscience and Biotechnology, Konkuk University, Seoul 143-701, Republic of Korea.*

† Corresponding author, E-mail: jwjung@sejong.ac.kr

Electronic Supplementary Information (ESI) available: [details of any supplementary information available should be included here]. See DOI: 10.1039/b000000x/

Reference

1. B. Radisavljevic, A. Radenovic, J. Brivio, V. Giacometti and A. Kis, *Nat Nanotechnol*, 2011, **6**, 147-150.
2. S. Bertolazzi, J. Brivio and A. Kis, *ACS nano*, 2011, **5**, 9703-9709.
3. D. Xiao, G.-B. Liu, W. Feng, X. Xu and W. Yao, *Physical review letters*, 2012, **108**, 196802.
4. K. F. Mak, K. He, J. Shan and T. F. Heinz, *Nat Nanotechnol*, 2012, **7**, 494-498.
5. Y. H. Chang, C. T. Lin, T. Y. Chen, C. L. Hsu, Y. H. Lee, W. Zhang, K. H. Wei and L. J. Li, *Advanced Materials*, 2013, **25**, 756-760.
6. Y. Yu, S.-Y. Huang, Y. Li, S. N. Steinmann, W. Yang and L. Cao, *Nano letters*, 2014, **14**, 553-558.
7. Q. Xiang, J. Yu and M. Jaroniec, *Journal of the American Chemical Society*, 2012, **134**, 6575-6578.
8. W. Zhou, Z. Yin, Y. Du, X. Huang, Z. Zeng, Z. Fan, H. Liu, J. Wang and H. Zhang, *Small*, 2013, **9**, 140-147.
9. M. Chhowalla, H. S. Shin, G. Eda, L.-J. Li, K. P. Loh and H. Zhang, *Nature chemistry*, 2013, **5**, 263-275.
10. D. Voiry, H. Yamaguchi, J. Li, R. Silva, D. C. Alves, T. Fujita, M. Chen, T. Asefa, V. B. Shenoy and G. Eda, *Nat Mater*, 2013, **12**, 850-855.
11. Y. Li, H. Wang, L. Xie, Y. Liang, G. Hong and H. Dai, *Journal of the American Chemical Society*, 2011, **133**, 7296-7299.
12. B. Hinnemann, P. G. Moses, J. Bonde, K. P. Jørgensen, J. H. Nielsen, S. Horch, I. Chorkendorff and J. K. Nørskov, *Journal of the American Chemical Society*, 2005, **127**, 5308-5309.
13. T. F. Jaramillo, K. P. Jørgensen, J. Bonde, J. H. Nielsen, S. Horch and I. Chorkendorff, *Science*, 2007, **317**, 100-102.
14. J. N. Coleman, M. Lotya, A. O'Neill, S. D. Bergin, P. J. King, U. Khan, K. Young, A. Gaucher, S. De and R. J. Smith, *Science*, 2011, **331**, 568-571.
15. A. Serov and C. Kwak, *Applied Catalysis B: Environmental*, 2010, **97**, 1-12.
16. J. Ma, N. A. Choudhury and Y. Sahai, *Renewable and Sustainable Energy Reviews*, 2010, **14**, 183-199.
17. K. Yamada, K. Yasuda, N. Fujiwara, Z. Siroma, H. Tanaka, Y. Miyazaki and T. Kobayashi, *Electrochemistry Communications*, 2003, **5**, 892-896.
18. J. Li, W. Tang, J. Huang, J. Jin and J. Ma, *Catalysis Science & Technology*, 2013, **3**, 3155-3162.
19. J. Li, W. Tang, H. Yang, Z. Dong, J. Huang, S. Li, J. Wang, J. Jin and J. Ma, *RSC Advances*, 2014, **4**, 1988-1995.
20. L. Q. Ye, Z. P. Li, H. Y. Qin, J. K. Zhu and B. H. Liu, *Journal of Power Sources*, 2011, **196**, 956-961.
21. X. Zhong, H. Yang, S. Guo, S. Li, G. Gou, Z. Niu, Z. Dong, Y. Lei, J. Jin and R. Li, *J. Mater. Chem.*, 2012, **22**, 13925-13927.
22. D. H. Dahanayaka, J. X. Wang, S. Hossain and L. A. Bumm, *Journal of the American Chemical Society*, 2006, **128**, 6052-6053.
23. A. El Kasmi, M. C. Leopold, R. Galligan, R. T. Robertson, S. S. Saavedra, K. El Kacemi and E. F. Bowden, *Electrochemistry Communications*, 2002, **4**, 177-181.
24. J. Zhang and M. Oyama, *Analytica chimica acta*, 2005, **540**, 299-306.
25. G. Chang, J. Zhang, M. Oyama and K. Hirao, *The Journal of Physical Chemistry B*, 2005, **109**, 1204-1209.
26. G. Chang, M. Oyama and K. Hirao, *The Journal of Physical Chemistry B*, 2006, **110**, 1860-1865.
27. J. Liu, C. Zhong, X. Du, Y. Wu, P. Xu, J. Liu and W. Hu, *Electrochimica Acta*, 2013, **100**, 164-170.
28. P. Qin, G. Fang, W. Ke, F. Cheng, Q. Zheng, J. Wan, H. Lei and X. Zhao, *Journal of Materials Chemistry A*, 2014, **2**, 2742-2756.
29. C. Muratore, J. Hu, B. Wang, M. Haque, J. Bultman, M. Jespersen, P. Shamberger, M. McConney, R. Naguy and A. Voevodin, *Applied Physics Letters*, 2014, **104**, 261604.
30. H. Li, Q. Zhang, C. C. R. Yap, B. K. Tay, T. H. T. Edwin, A. Olivier and D. Baillargeat, *Advanced Functional Materials*, 2012, **22**, 1385-1390.
31. X. Luo, Y. Zhao, J. Zhang, Q. Xiong and S. Y. Quek, *Physical Review B*, 2013, **88**, 075320.
32. Y. Yu, C. Li, Y. Liu, L. Su, Y. Zhang and L. Cao, *Scientific reports*, 2013, **3**.
33. A. Gurarslan, Y. Yu, L. Su, Y. Yu, F. Suarez, S. Yao, Y. Zhu, M. Ozturk, Y. Zhang and L. Cao, *ACS nano*, 2014.
34. K.-K. Liu, W. Zhang, Y.-H. Lee, Y.-C. Lin, M.-T. Chang, C.-Y. Su, C.-S. Chang, H. Li, Y. Shi and H. Zhang, *Nano letters*, 2012, **12**, 1538-1544.
35. G.-W. Yang, G.-Y. Gao, C. Wang, C.-L. Xu and H.-L. Li, *Carbon*, 2008, **46**, 747-752.
36. H. Gao, Y. Wang, F. Xiao, C. B. Ching and H. Duan, *The Journal of Physical Chemistry C*, 2012, **116**, 7719-7725.
37. W. Ye, B. Yang, G. Cao, L. Duan and C. Wang, *Thin solid films*, 2008, **516**, 2957-2961.
38. Q. Yi and W. Yu, *Journal of Electroanalytical Chemistry*, 2009, **633**, 159-164.
39. C. Muratore, J. Hu, B. Wang, M. Haque, J. Bultman, M. Jespersen, P. Shamberger, M. McConney, R. Naguy and A. Voevodin, *Applied Physics Letters*, 2014, **104**, 261604.